Figure 2B (curve i) shows an example of the computed Allan deviation for the frequency comparison (method of Fig. 1B) between BIPM-C2 and NIST-BB1 at 456 THz. The very low Allan deviation of $\sim 2.3 \times 10^{-17}$ at 1 s is achieved when the beams from the two femtosecond lasers are made to be mostly collinear with the 456-THz laser that controls each synthesizer. This implies that the path length fluctuations from the two synthesizers to the heterodyne photodetector are common mode at an approximate level of <10 nm in 1 s of averaging. This low instability enables us to reach statistical uncertainties as low as a few parts in 10^{19} with less than 1000 s of averaging (Fig. 2B). Also shown in Fig. 2B are Allan deviations from other optical and microwave frequency synthesizers.

Figure 3 shows the short-term (1 s) and averaged uncertainties obtained from our measurements, along with measured and projected uncertainties associated with the laser control systems, Doppler shifts, and fundamental shot noise. The short-term (1 s) uncertainty arises from differential mechanical vibrations and variations in air pressure and temperature. The estimated level of these fluctuations (Fig. 3, line i) is in agreement with the measurements across the optical spectrum, except near the frequency $f_L = 456$ THz where we could arrange the optical paths collinearly for maximum common-mode suppression. The limit set by the performance of the laser control (Fig. 3, line ii) is only a factor of 1.5 below the 1-s uncertainty near 456 THz. The estimated shot noise–limited uncertainty at 1-s averaging for the control of the femtosecond laser synthesizer relative to f_L is shown in Fig. 3, line iii.

Instabilities on longer time scales or frequency offsets that result in systematic errors are of greater concern. In our comparisons, the various synthesizers were separated by ~ 2 m on a steel table. With temperature variations of $\sim 0.1°C$ per hour, the thermal expansion of the steel results in a fractional Doppler shift on the order of a few parts in 10^{18}. We have attempted to cancel this effect by arranging the optical paths for our experiments in a symmetric fashion with as much common-mode rejection as possible. In addition, the relatively long data acquisition times of several hours provide some immunity by averaging over temperature fluctuations on the 100- to 1000-s time scale. In principle, the control system compensates for all Doppler shifts inside the control loop path at frequency $f_L = 456$ THz; however, because of dispersion (or physically different paths) this is not the case for the emitted frequencies far from f_L. For example, if the nonlinear optical fiber in BIPM-C2 and ECNU-C1 expands at the same rate given above, the resulting Doppler shift for the frequencies near 333 THz is ~ 200 μHz, which corresponds to a fractional shift of 5×10^{-19} (Fig. 3, line iv). This indicates that longer averaging times ($\geq 100,000$ s) or direct mea-

surement and compensation of all Doppler shifts would be required to reduce the uncertainty below the level of 10^{-19}.

Considering the very different designs of these synthesizers (broadband operation versus nonlinear microstructure fiber), it is notable that our data do not point to the existence of any fundamental limitations to the uncertainty. Our results appear to be limited mainly by noise of a technical nature (thermal and mechanical fluctuations) and total integration time. The reproducibility demonstrated in our experiments firmly establishes the femtosecond laser synthesizer as a reliable tool for optical frequency comparisons with uncertainties approaching 10^{-19}, and demonstrates its value for precision measurements in experimental physics.

References and Notes
1. P. Gill, Ed., *Proceedings of the 6th Symposium on Frequency Standards and Metrology* (World Scientific, Singapore, 2002).
2. S. A. Diddams *et al.*, *Science* **293**, 825 (2001).
3. J. Ye, L.-S. Ma, J. Hall, *Phys. Rev. Lett.* **87**, 270801 (2001).
4. B. C. Young, F. C. Cruz, W. M. Itano, J. C. Bergquist, *Phys. Rev. Lett.* **82**, 3799 (1999).
5. C. W. Oates, E. A. Curtis, L. Hollberg, *Opt. Lett.* **25**, 1603 (2000).
6. H. G. Dehmelt, *IEEE Trans. Instrum. Meas.* **31**, 83 (1982).
7. S. G. Karshenboim, *Can. J. Phys.* **78**, 639 (2000).
8. J. D. Prestage, R. J. Tjoelker, L. Maleki, *Phys. Rev. Lett.* **74**, 3511 (1995).
9. H. Marion *et al.*, *Phys. Rev. Lett.* **90**, 150801 (2003).
10. S. Bize *et al.*, *Phys. Rev. Lett.* **90**, 150802 (2003).
11. J. K. Webb *et al.*, *Phys. Rev. Lett.* **87**, 091301 (2001).
12. J. N. Eckstein, A. I. Ferguson, T. W. Hänsch, *Phys. Rev. Lett.* **40**, 847 (1978).
13. Th. Udem, R. Holzwarth, T. W. Hänsch, *Nature* **416**, 233 (2002).
14. Th. Udem, J. Reichert, R. Holzwarth, T. W. Hänsch, *Phys. Rev. Lett.* **82**, 3568 (1999).
15. Th. Udem, J. Reichert, R. Holzwarth, T. W. Hänsch, *Opt. Lett.* **24**, 881 (1999).
16. R. Holzwarth *et al.*, *Phys. Rev. Lett.* **85**, 2264 (2000).
17. S. A. Diddams *et al.*, *Opt. Lett.* **27**, 58 (2002).
18. J. Stenger *et al.*, *Phys. Rev. Lett.* **88**, 073601 (2002).
19. M. Zimmermann *et al.*, *Opt. Lett.* **29**, 310 (2004).
20. See supporting data on *Science* Online.
21. R. K. Shelton *et al.*, *Science* **293**, 1286 (2001).
22. I. Lira, *Evaluating the Measurement Uncertainty* (Institute of Physics, Bristol, UK, 2002).
23. D. W. Allan, *IEEE Trans. Ultrason. Ferroelect. Freq. Control* **34**, 647 (1987).
24. A. Sen Gupta, D. Popovic, F. L. Walls, in *Proceedings of the 1999 Joint Meeting of the European Frequency and Time Forum (EFTF) and the IEEE International Frequency Control Symposium (FCS)*, Besançon, France, 13 to 16 April 1999 (IEEE, Piscataway, NJ, 1999), pp. 615–619.
25. A. Bartels, S. A. Diddams, T. M. Ramond, L. Hollberg, *Opt. Lett.* **28**, 663 (2002).
26. We thank T. Ramond, R. Fox, and J. Bergquist for their contributions to this work, and J. Hall, D. Wineland, and J. Ye for their thoughtful comments on this manuscript. The work at NIST was funded in part by NASA. The project at ECNU was funded in part by the Science and Technology Commission of Shanghai Municipality (01DJGK014, 022261033), Shanghai Municipal Education Commission, National Science Foundation of China (10274020), and Ministry of Education, China (02106).

A Molecular Elevator

Jovica D. Badjić,[1] Vincenzo Balzani,[2] Alberto Credi,[2]* Serena Silvi,[2] J. Fraser Stoddart[1]*

We report the incrementally staged design, synthesis, characterization, and operation of a molecular machine that behaves like a nanoscale elevator. The operation of this device, which is made of a platformlike component interlocked with a trifurcated riglike component and is only 3.5 nanometers by 2.5 nanometers in size, relies on the integration of several structural and functional molecular subunits. This molecular elevator is considerably more complex and better organized than previously reported artificial molecular machines. It exhibits a clear-cut on-off reversible behavior, and it could develop forces up to around 200 piconewtons.

Biomotor molecules are extremely complex machines, the detailed structures and precise working mechanisms of which have been elucidated only in a very few cases (*1*, *2*). Chemists are trying to construct much simpler molecular machines as a logical step toward mimicking the actions of biomotor molecules (*3–5*). In the past few years, several different kinds (*6–14*) of artificial molecular machines have been designed and constructed.

Here, we describe the incrementally staged design, bottom-up construction, characterization, and chemically driven operation of a two-component molecular machine that behaves like a nanometer-scale elevator. This nanoactuator, which is circa (ca.) 2.5 nm in height with diameter of ca. 3.5 nm, consists of a trifurcated riglike

[1]California NanoSystems Institute and Department of Chemistry and Biochemistry, University of California, Los Angeles, 405 Hilgard Avenue, Los Angeles, CA 90095, USA. [2]Dipartimento di Chimica "G. Ciamician," Università di Bologna, Via Selmi 2, 40126 Bologna, Italy.

*To whom correspondence should be addressed. E-mail: alberto.credi@unibo.it (A.C.); stoddart@chem.ucla.edu (J.F.S.)

component containing two different notches at different levels in each of its three legs that are interlocked by a platform. The platform is made up of loops in the form of three macrocycles, fused trigonally to a central floor, that can be made to stop at the two different levels. The three legs of the rig carry bulky feet that prevent the loss of the platform. The energy needed to raise and lower the platform between the two levels on the rig's legs is supplied by an acid-base reaction. The distance traveled by the platform is about 0.7 nm, and we estimate that the elevator movement from the upper to lower level could generate a force of up to 200 pN.

The molecular elevator has its origin in the molecular shuttle, a degenerate two-station [2]rotaxane (15). The promise of this mechanically interlocked molecule (16) to act as the prototype for the construction of linear motors, based on highly controllable [2]rotaxanes, has been realized recently by redox (8, 11, 12), acid-base (8), and photochemical (11, 13) stimulations. In such systems, a ring component encircles preferentially one of two recognition sites present along the rodlike section of a dumbbell-shaped component. It is possible then (Fig. 1A), by using an appropriate external stimulus, to induce the ring to move in an almost linear fashion from one station to the other. Redox-controllable bistable [2]rotaxanes have already been incorporated as electronically reconfigurable switches into both simple memory and logic circuits (17).

Previously, we have described (8, 18) the acid-base switching (Fig. 1B) of the [2]rotaxane $[1H]^{3+}$ composed of a dumbbell-shaped component containing two different stations, namely, a dialkylammonium $(-NH_2^+-)$ center and a bipyridinium $(BIPY^{2+})$ unit, encircled by a dibenzo[24]crown-8 (DB24C8) ring component. We demonstrated, with the use of a variety of techniques, that in both acetone and acetonitrile the DB24C8 ring resides almost exclusively around the $-NH_2^+-$ center in one of the two possible translationally isomeric forms. X-ray crystallography has revealed (19) that this preference results from a combination of strong $[N^+-H\cdots O]$ hydrogen bonding and weak $[C-H\cdots O]$ interactions, augmented more often than not with some stabilizing $[\pi\text{-}\pi]$ stacking forces. On addition of a base (a tertiary amine) to a solution of $[1H]^{3+}$, deprotonation of the $-NH_2^+-$ center occurs. The strong intercomponent hydrogen bonding is destroyed, and the DB24C8 ring moves to the $BIPY^{2+}$ unit, where it is stabilized by $[C-H\cdots O]$ and $[\pi\text{-}\pi]$ stacking interactions. Subsequent addition of acid restores the $-NH_2^+-$ center, and the DB24C8 ring moves back to encircle this recognition site. The shuttling process, which

can be followed by nuclear magnetic resonance (^1H NMR) spectroscopy and electrochemical techniques, is quantitative (8).

In pursuit of a better fundamental understanding of the nature of multivalency (20) in polytopic hosts and guests, we investigated (21) the acid-base–controlled (Fig. 1C) assembly and disassembly of a triply threaded two-component superbundle. This 1:1 adduct consists of a tritopic host **2**, in which three DB24C8 rings are fused together within a triphenylene core, and a trifurcated guest trication $[3H_3]^{3+}$ wherein three dibenzylammonium ions are linked to a central benzenoid core. Fluorescence titration experiments (including Job plots), as well as electrochemical and ^1H NMR spectroscopic data, have established the remarkable strength of the superbundle encompassing the triply expressed binding motif revealed by x-ray crystallography in the solid state (21). In acetonitrile solution, the dethreading and rethreading of the 1:1 adduct can be controlled by addition of base and acid.

By incorporating the architectural features (Fig. 1B) of the acid-base switchable [2]rotaxane $[1H]^{3+}/1^{2+}$ into those (Fig. 1C) of the trifurcated trication $[3H_3]^{3+}$, we came up with the design of the molecular elevator shown in Fig. 2. It was synthesized with the use of a template-directed protocol (22) from the trifurcated guest salt $[4H_3][PF_6]_6$ and the tritopic host **2**, which form a 1:1 adduct (superbundle) that can be converted into a mechanically interlocked elevator $[5H_3]^{9+}$ by functionalization of the ends of each leg with bulky 3,5-di-*tert*-butylbenzyl feet

(scheme S1). This compound, and its model $[6H_3]^{9+}$, which were both isolated as their $9PF_6^-$ salts, were characterized by ^1H NMR spectroscopy, electrochemistry, and absorption and fluorescence spectroscopy.

The ^1H NMR spectrum (Fig. 3A) of $[5H_3][PF_6]_9$ in CD_3CN exhibits a complex array of resonances corresponding to a triply threaded, mechanically interlocked molecule with averaged C_{3v} symmetry. Characteristic (18) downfield shifts of the methylene proton resonances next to the $-NH_2^+-$ centers indicate the preferred binding of the platform's three crown ether loops with the three $-NH_2^+-$ centers in the legs of the rig. No additional proton resonances were obtained in the ^1H NMR spectrum when a CD_3COCD_3 solution of $[5H_3][PF_6]_9$ was cooled down to $-80°C$. These observations confirm that $[5H_3]^{9+}$ exists in the co-conformation shown in Fig. 3D. Addition of a strong, nonnucleophilic phosphazene base to a solution of the elevator in CD_3CN caused dramatic changes in the ^1H NMR spectrum, particularly in the chemical shifts of the $BIPY^{2+}$ and *p*-xylyl methylene protons, demonstrating that the three crown ether loops on the platform are now associated with the three $BIPY^{2+}$ recognition sites. The addition of <3 equivalents of base led to the extensive line broadening, indicating the presence of several slowly exchanging intermediate co-conformations on the ^1H NMR time scale, whereas, after addition (Fig. 3B) of a slight excess (3.4 equivalents), only the hexacationic species 5^{6+}, in which the elevator

Fig. 1. (A) Schematic representation of a controllable, bistable [2]rotaxane, containing in its dumbbell-shaped component two different recognition sites or "stations," to one of which the ring component is attracted much more than the other. The two different states of the molecule can be switched by an external stimulus, such as a change in pH. **(B)** In the [2]rotaxane $[1H]^{3+}$, the dumbbell-shaped component contains a $-NH_2^+-$ center and a $BIPY^{2+}$ unit as sta-

tions for the DB24C8 component (8). In acid, the preferred station for the DB24C8 ring to encircle is the $-NH_2^+-$ center because of the formation of strong hydrogen bonds. On addition of base, however, the $-NH_2^+-$ center is deprotonated and the DB24C8 moves to the $BIPY^{2+}$ unit, where the donor-acceptor interactions become stabilizing. **(C)** The equilibrium between the tris-crown ether **2** and the tris-ammonium ion $[3H_3]^{3+}$, which lies very much to the right in favor of the superbundle in solvents such as acetonitrile and dichloromethane (21). The graphical representation of the superbundle portrays the good surface-to-surface match between the two interpenetrating components. The dots indicate the $[N^+-H\cdots O]$ hydrogen bonds between the $-NH_2^+-$ centers of $[3H_3]^{3+}$ and the fused DB24C8 rings in **2**, and the horizontal dashes, the $[\pi\text{-}\pi]$ stacking interactions between the central aromatic cores. The superbundle can be disassembled by addition of a base and reassembled by addition of an acid.
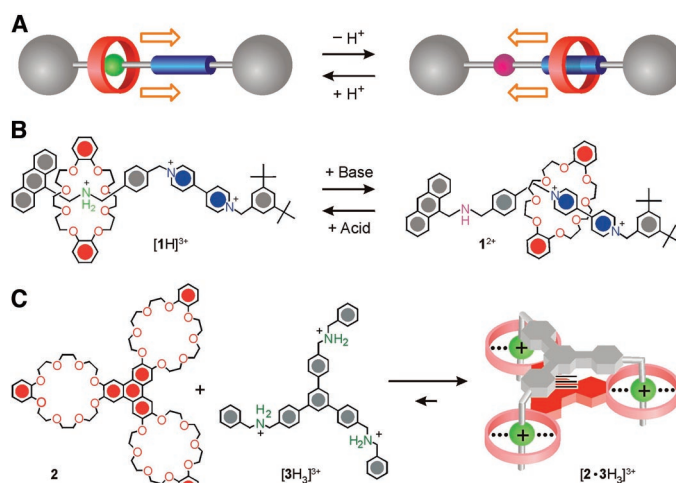
has reached the lower level, is present. The original ^{1}H NMR spectrum was regenerated in every detail on addition of a slight excess of trifluoroacetic acid to the NMR sample treated with the base; i.e., the elevator goes back completely to the upper level.

Clear evidence for the elevator operating with base and acid inputs was also obtained from electrochemical experiments performed in acetonitrile solution. It is well known (23) that BIPY^{2+} units undergo two successive, reversible monoelectronic reduction processes at about −0.4 and −0.8 V [compared with a saturated calomel electrode (SCE)]. When BIPY^{2+} units are surrounded by electron donors such as the catechol rings in DB24C8, their reduction potentials become displaced (8) to more negative values by about 150 to 200 mV. We found that $[\mathbf{6}H_3]^{9+}$ (Fig. 2) exhibits two successive reversible three-electron reduction processes at −0.35 V and −0.80 V, indicating that the three BIPY^{2+} units (i) are equivalent, (ii) behave independently of one another, and (iii) are not engaged in electron donor-acceptor interactions. On deprotonation of the control $[\mathbf{6}H_3]^{9+}$ by addition of the phosphazene base, the two reduction waves (Fig. 4A) are almost unaffected. The electrochemical behavior of the molecular elevator $[\mathbf{5}H_3]^{9+}$ is quite similar to that of the control $[\mathbf{6}H_3]^{9+}$, indicating that the three BIPY^{2+} units are not interacting with the electron-donating catechol rings at the periphery of the platform. Thus, the initial co-conformation adopted by $[\mathbf{5}H_3]^{9+}$ corresponds to the one in which the crown ether loops on the platform all surround the −NH$_2^+$− centers on the three-legged rig (on the upper level). On addition of slightly more than 3 equivalents of base, however, the two reduction waves are displaced (Fig. 4A) to more negative potentials, indicating that the three BIPY^{2+} units in the three legs, although remaining equivalent and independent from one another, are now surrounded by the
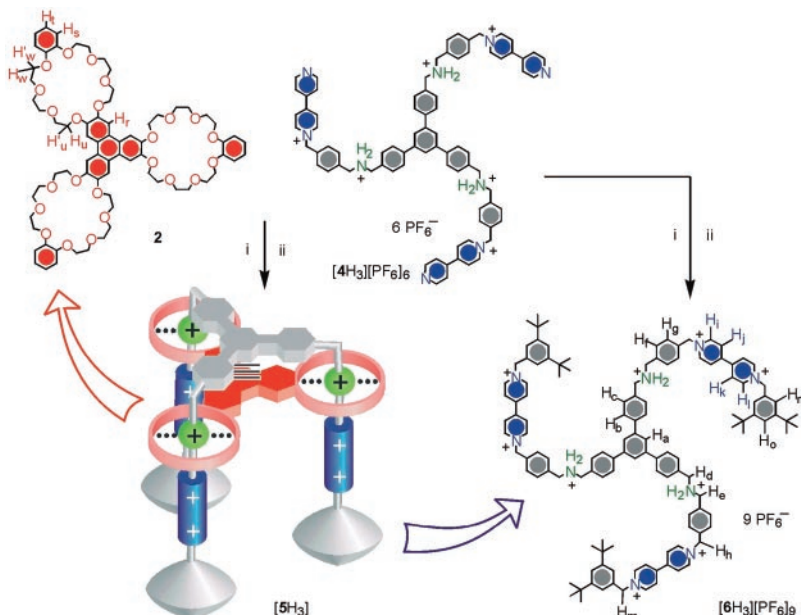

Fig. 2. The trifurcated guest salt $[\mathbf{4}H_3][PF_6]_6$ and the tritopic host **2** (each 6.6 mM) in a CHCl$_3$/MeCN solution (3.0 mL, 2:1) form a 1:1 adduct (superbundle) that was, at elevated temperature (75°C), converted to the mechanically interlocked elevator $[\mathbf{5}H_3][PF_6]_9$ in the reaction with (i) 3,5-di-*tert*-butylbenzylbromide(200 mM), followed by (ii) the counterion-exchange (NH$_4$PF$_6$/MeOH/H$_2$O). Following the same protocol, only without **2**, the model compound $[\mathbf{6}H_3][PF_6]_9$ was synthesized.
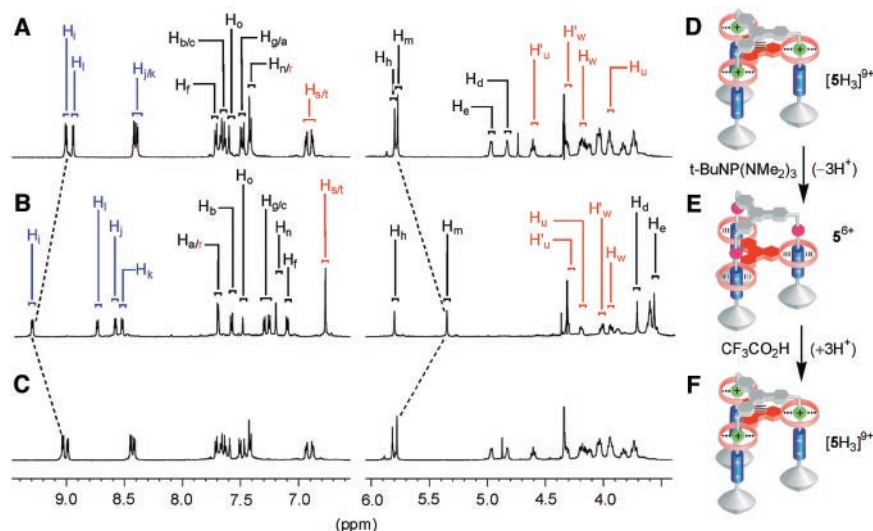

Fig. 3. ^{1}H NMR spectra (600 MHz, CD$_3$CN, 4.3 mM, and 298 K) recorded on $[\mathbf{5}H_3][PF_6]_9$ before (**A**) and after (**B**) addition of 3.4 equivalents of the phosphazene base, *N-t*-butyl-*N′,N′,N′′,N′′,N′′′,N′′′*-hexamethylphosphorimidic triamide. The original spectrum is regenerated (**C**) on addition of 3.4 equivalents of trifluoroacetic acid. The corresponding operation of the molecular elevator is shown on the right-hand side. The platform is situated on the upper level (**D**) at the outset. Addition of the base causes the platform to move to the lower level (**E**). Addition of acid restores the platform to the upper level (**F**).
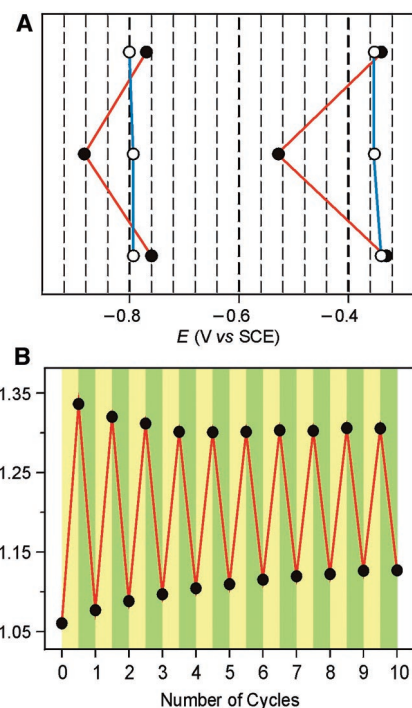

Fig. 4. (**A**) Potential values, in V versus SCE, for the reduction processes of the BIPY^{2+} units of $[\mathbf{5}H_3]^{9+}$ (●) and $[\mathbf{6}H_3]^{9+}$ (○) (top) on addition of a base to afford $\mathbf{5}^{6+}$ and, respectively, $\mathbf{6}^{6+}$ (middle) and after reprotonation with an acid, a stoichiometric amount with respect to the added base (bottom). (**B**) Changes in absorbance observed at 310 nm (path length is 4.0 cm) for a 7.1 μM solution of $[\mathbf{5}H_3]^{9+}$ on successive addition of stoichiometric amounts of base (yellow areas) and acid (green areas). All experiments were carried out in acetonitrile solution at 298 K.

electron-donating crown ether loops of the platform. The changes in reduction potential can be fully reversed by addition of acid, and the cycle can be repeated without any significant loss of reversibility.

The chemically driven operation of the molecular elevator $[5H_3]^{9+}$ also leads to reversible changes in the emission and absorption spectra. In acetonitrile solution, $[5H_3]^{9+}$ exhibits a relatively weak emission band with a maximum at ca. 380 nm. On successive additions of stochiometric amounts of the base and acid, the intensity of the band increases and, respectively, decreases. This behavior is also witnessed in the absorption spectrum. The change in absorbance at 310 nm on successive additions of base and acid shows (Fig. 4B) that the process can be repeated several times, with some loss of signal in the first cycles.

The current intensities of the cyclic voltammetric peaks of the "free" and "complexed" BIPY^{2+} units decrease and, respectively, increase linearly on addition of 1, 2, and 3 equivalents of base (Fig. 5A). These data do not, however, shed any light on the precise mechanism of the platform's operation, i.e., whether the addition of 1 equivalent of base forms exclusively the species with only one loop displaced, or a statistical distribution of species with none, one, two, or three loops displaced. We therefore performed titration experiments and monitored changes in absorption spectra. A plot (Fig. 5B) of the absorbance changes (e.g., at 276 nm) on titration of $[5H_3]^{9+}$ with base shows the pres-

ence of three quite distinct steps, indicating that the three deprotonation processes are not equivalent. Thus, addition of the first equivalent of base does not lead to a statistical mixture of differently protonated species but rather causes the first deprotonation process to occur, first of all, in all $[5H_3]^{9+}$ ions, and so on. Molecular modeling (Fig. 5C) shows that the species in which two (or one) loop(s) surround (a) –NH$_2$$^+$– center(s) and one (or two) loop(s) surround(s) (a) BIPY^{2+} unit(s) are sterically possible. And so, for each $[5H_3]^{9+}$, the platform operates in three discrete steps associated with each of the three deprotonation processes that take $[5H_3]^{9+}$ progressively through $[5H_2]^{8+}$ and $[5H]^{7+}$ ions to, finally, 5^{6+}.

From thermodynamic considerations, it can be established [Supporting Online Material (SOM) Text] that the energies available for the relevant movements from the upper to lower levels (base stroke) and from the lower to upper levels (acid stroke) amount to ca. 21 and >4 kcal mol^{-1}, respectively. These large stabilization energies not only provide strong driving forces for the molecular motion, they also confer a high positional (co-conformational) integrity on the elevator, giving rise to a clear-cut on-off behavior. Because the distance traveled by the platform is about 0.7 nm, the nanoactuator can potentially generate a force of up to 200 pN in the motion from the upper to the lower level. Such force is more than one order of magnitude larger than those developed (2) by natural linear motors like myosin and kinesin.

The bundle $[5H_3]^{9+}$, besides operating as a molecular elevator, could also serve other useful functions. The movement of the platform from the upper level, in which the loops surround the –NH$_2$$^+$– centers on the legs, to the lower level, where the loops surround the BIPY^{2+} units, opens up a potentially large cavity (1.5 nm by 0.8 nm) in 5^{6+} that is closed down again when the system returns to the upper level (Fig. 5C). Such a cavity, whose sides contain three amine functions and whose floor and roof are defined by aromatic rings, could play host to some large guest molecules. Additionally, the base-acid control mechanism might be accompanied by the switching "on" and "off" of a potentially attractive hosting capacity. We also note that, when the platform is on the upper level, the three BIPY^{2+} units are not engaged in any interactions and so the elevator is free to move its legs, whereas, when the platform is at the lower level, these same legs will be rigidified as well as occupied. Thus, when the platform is on the upper level, the BIPY^{2+} units could form adducts with other electron donor species present in the solution, whereas this possibility is precluded when the platform resides at the lower level. Also, because the BIPY^{2+} units lose their electron-accepting character upon reduction (6, 7, 23), the adduct-forming capacity of the three BIPY^{2+} legs could also be controlled electrochemically.

The molecular elevator has a complex structure that is capable of performing well-defined mechanical movements under the actions of external inputs; i.e., it is possible to produce multivalent compounds (24) capable of performing nontrivial mechanical movements and exercising a variety of different functions on external stimulation.

References and Notes

1. G. Oster, H. Wang, *Trends Cell Biol.* **13**, 114 (2003).
2. M. Schliwa, G. Woehlke, *Nature* **422**, 759 (2003).
3. Structural and functional integration of motor proteins within artificial nanodevices has also been obtained. For examples, see (4) and (5).
4. G. Steinberg-Yfrach et al., *Nature* **392**, 479 (1998).
5. R. K. Soong et al., *Science* **290**, 1555 (2000).
6. V. Balzani, A. Credi, F. M. Raymo, J. F. Stoddart, *Angew. Chem. Int. Ed. Engl.* **39**, 3348 (2000).
7. V. Balzani, A. Credi, M. Venturi, *Molecular Devices and Machines – A Journey into the Nano World* (Wiley-VCH, Weinheim, Germany, 2003).
8. P. R. Ashton et al., *J. Am. Chem. Soc.* **120**, 11932 (1998).
9. T. R. Kelly, H. De Silva, R. A. Silva, *Nature* **401**, 150 (1999).
10. N. Koumura, R. W. Zijlstra, R. A. van Delden, N. Harada, B. L. Feringa, *Nature* **401**, 152 (1999).
11. P. R. Ashton et al., *Chem. Eur. J.* **6**, 3558 (2000).
12. J.-P. Collin, C. O. Dietrich-Buchecker, P. Gaviña, M. C. Jimenez-Molero, J.-P. Sauvage, *Acc. Chem. Res.* **34**, 477 (2001).
13. A. M. Brouwer et al., *Science* **291**, 2124 (2001); published online 22 February 2001 (10.1126/science.1057886).
14. D. A. Leigh, J. K. Y. Wong, F. Dehez, F. Zerbetto, *Nature* **424**, 174 (2003).
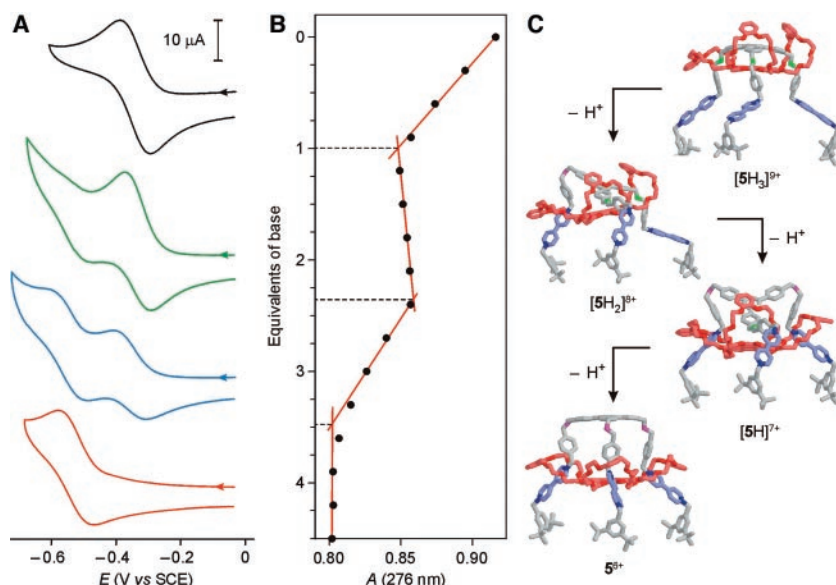
Fig. 5. (A) Cyclic voltammetric curves for the first three-electron reduction of (from top to bottom) $[5H_3]^{9+}$, $[5H_2]^{8+}$, $[5H]^{7+}$, and 5^{6+}. Conditions were a 0.40 mM molecular elevator, acetonitrile solution with 0.04 M tetraethylammonium hexafluorophosphate as supporting electrolyte, 100 mV s^{-1}, glassy carbon electrode, 298 K. **(B)** Changes in the absorbance at 276 nm on titration of $[5H_3]^{9+}$ with the phosphazene base in 5.0 μM acetonitrile solution at 298 K. **(C)** Stepwise motion of the platform down to the legs of the rig on successive deprotonation of its three –NH$_2$$^+$– centers. The structures shown were obtained by molecular mechanics calculations.

15. P. L. Anelli, N. Spencer, J. F. Stoddart, *J. Am. Chem. Soc.* **113**, 5131 (1991).
16. J.-P. Sauvage, C. Dietrich-Buchecker, Eds., *Molecular Catenanes, Rotaxanes and Knots* (VCH-Wiley, Weinheim, Germany, 1999).
17. Y. Luo *et al.*, *ChemPhysChem* **3**, 519 (2002).
18. M.-V. Martínez-Díaz, N. Spencer, J. F. Stoddart, *Angew. Chem. Int. Ed.* **36**, 1904 (1997).
19. S. J. Cantrill, A. R. Pease, J. F. Stoddart, *J. Chem. Soc. Dalton Trans.* **21**, 3715 (2000).
20. M. Mammen, S.-K. Choi, G. M. Whitesides, *Angew. Chem. Int. Ed. Engl.* **37**, 2754 (1998).
21. V. Balzani *et al.*, *Chem. Eur. J.* **9**, 5348 (2003).
22. S. Anderson, H. L. Anderson, J. K. M. Sanders, *Acc. Chem. Res.* **26**, 469 (1993).
23. P. M. S. Monk, *The Viologens. Physicochemical Properties, Synthesis and Application of the Salts of 4,4′-Bipyridine* (Wiley, Chichester, UK, 1998).
24. Although multivalency is a concept that is well-established with regard to numerous biological

systems, its investigation has been restricted largely to the acquisition of thermodynamic parameters, e.g., association or dissociation constants and free energies, enthalpies, and entropies of complexation. In the present investigation, the opportunity arose to study within a molecularly constrained environment how three equivalent recognition sites respond to being addressed chemically. The fact that they switch in series rather than in parallel is a feature worthy of note. Although many might argue intuitively that multivalency from a mechanistic standpoint has to be a stepwise process, the results presented in this article provide indirect yet convincing experimental evidence for the one-at-a-time mechanism; i.e., by taking single steps rather than moving in concert, the molecular elevator is more reminiscent of a legged animal than it is of the passenger elevator.

Electrical or Photocontrol of the Rotary Motion of a Metallacarborane

M. Frederick Hawthorne,[1]* Jeffrey I. Zink,[1] Johnny M. Skelton,[1] Michael J. Bayer,[1] Chris Liu,[1] Ester Livshits,[2] Roi Baer,[2] Daniel Neuhauser[1]

Rotary motion around a molecular axis has been controlled by simple electron transfer processes and by photoexcitation. The basis of the motion is intramolecular rotation of a carborane cage ligand (7,8-dicarbollide) around a nickel axle. The Ni(III) metallacarborane structure is a *transoid* sandwich with two pairs of carbon vertices reflected through a center of symmetry, but that of the Ni(IV) species is *cisoid*. The interconversion of the two provides the basis for controlled, rotational, oscillatory motion. The energies of the Ni(III) and Ni(IV) species are calculated as a function of the rotation angle.

The smallest nanomachines made to date are based on changes in molecular bonding. In biological motors, such as those that power the linear motion of myosin head in muscle contraction (*1, 2*) or the rotary motion of F_1-adenosine triphosphatase (*3–5*) in bacterial flagella, the hydrolysis energy of the adenosine triphosphate (ATP) to diphosphate reaction creates new bonds that can exert forces that change the shape of the larger molecule and perform work.

Given the existence of biological motors, the interest of chemists in designing molecular motors stems from the challenge not only of making even smaller nanomachines that perform controllable motion (*6*), but also of creating systems that can be powered with light or electrical energy, rather than depending on the delivery of ATP. Linear motors have been developed such as the rotaxane systems (*7–9*), in which a shuttle ring component slides from one physically discrete zone of a rigid rod to another.

Assessing a potential molecular motor based on changes in bonding must include determining whether the system has well-defined reactant and product states that are separated by a considerable energy barrier. The reasons are twofold. First, there has to be some way of putting into the molecule energy that will be recovered later as work. For photon-driven systems, this would likely be an excited state; for electrically driven systems, this could be the formation of an intermediate with a different redox state. Second, in either case, the product formed must have a barrier against back reaction, or it is unlikely that the system would exert any force; it would more likely relax back unproductively to the reactant configuration.

With these configurations in mind, we reexplored a small metal complex with potential as a two-state rotary machine that could be used, for example, to open or close a valve or switch. Examples to date of artificial rotors have been few. Rotary motion in synthetic arrays is represented by molecular windmills and turnstiles in which one component of the molecular device is capable of freewheeling rotation on a molecular axis (*10*), but such barrier-free unrestricted rotation cannot be powered or con-

trolled. The rotation of a dipolar rotor in a rotating electric field has been modeled (*11*). Examples in which control is possible are provided by the interlocked rings of catenanes that undergo circumrotation by passing through each other (*12, 13*). However, machines with rotary motion about a rigid molecular axis, controlled by simple electron transfer processes or by photoexcitation, have not been previously reported.

The basis of the molecular device reported here has been known since the discovery (*14*) of the d^7 Ni(III) and d^6 Ni(IV) *commo*-bis-7,8-dicarbollyl metallacarboranes, denoted as **1T** (*15*) and **1C** (*16*) (Fig. 1), and their palladium analogs. These complexes are produced by the coordination of two dicarbollide ions (*17*) (Fig. 1, **2**) with a Ni(II) ion, followed by subsequent oxidation. The "sandwich" species may undergo rotary motion of the ligands with respect to each other. This is analogous to the well-known metallocenes (*18*), but those have rotational barriers only of 2 kcal/mol (*19*.) The present metallacarboranes have barriers about three times as large, leading to temperature invariance in their nuclear magnetic resonance (NMR) spectra.

The presence of two adjacent CH vertices in the bonding face of **2** introduces localized regions of reduced negative charge (*20*) and an antipodal concentration of negative charge. The resulting interligand interaction leads to a *trans* configuration (*15, 17, 21*) (such as in **1T**) in most examples of *commo*-bis-7,8-dicarbollyl metallacarboranes. One of the few exceptions is the Ni(IV) species (**1C**), which is *cisoid*, with its pairs of carbon vertices on the same side of the molecule (*14, 15*). Nickel rarely appears in the formal +4 oxidation state in inorganic structures (*22*) and never in organometallic compounds, thereby making **1C** quite unusual.

The interconversion of the **1T** and **1C** geometries when the nickel oxidation state is changed provides the basis for the controlled, rotational, oscillatory motion and can be achieved electrochemically, by redox reactions, or photochemically. Thus, an oscillatory molecular rotor, providing useful work on the molecular scale, is plausible, based on the

[1]Department of Chemistry and Biochemistry, University of California, Los Angeles, CA, 90095–1569, USA. [2]Department of Chemistry, Hebrew University of Jerusalem, Givat Ram, Jerusalem, Israel.

*To whom correspondence should be addressed. E-mail: mfh@chem.ucla.edu